Int. J. Adv. Eng. Pure Sci. 2026, 38(1): <231-243>
DOI: 10.7240/jeps.1877813

RESEARCH ARTICLE / ARAŞTIRMA MAKALESİ

Design of a GO@AuNPs-embedded MIP-based electrochemical sensor for ceftazidime analysis

Ahmet ÇETİNKAYA [1], **Sibel A. ÖZKAN** [2]

[1]*University of Health Sciences, Gülhane Faculty of Pharmacy, Department of Analytical Chemistry, Ankara, Türkiye*

[2]*Ankara University, Faculty of Pharmacy, Department of Analytical Chemistry, Ankara, Turkiye*

Abstract

Ceftazidime (CTZ), a third-generation cephalosporin, is widely used to treat severe bacterial infections owing to its strong activity against Gram-negative pathogens. Accurate and sensitive determination of CTZ in biological and pharmaceutical matrices is of great importance for therapeutic drug monitoring and quality control. In this study, a molecularly imprinted polymer (MIP)–based electrochemical sensor was designed for the selective and ultrasensitive detection of CTZ. A graphene oxide/gold nanoparticle (GO@AuNPs) nanocomposite was used as the supporting matrix owing to its excellent electrical conductivity, large specific surface area, and synergistic signal amplification. The incorporation of this nanostructured platform significantly enhanced the sensor's electrochemical performance. Molecular recognition was achieved by constructing an MIP layer on the GO@AuNPs-modified electrode surface. The polymeric film was synthesized via photopolymerization (PP), which allows precise control of polymer structure and ensures structural uniformity under mild reaction conditions. Trans-3-(3-pyridyl)acrylic acid (3,3-PAA) was utilized as the functional monomer, selected for its strong and specific interactions with CTZ, thereby facilitating the formation of complementary recognition sites with high affinity and selectivity within the imprinted polymer network. Under optimized experimental conditions, the sensor exhibited a linear response in the range of 2.50×10^{-13} to 3.75×10^{-12} M, with a limit of detection (LOD) of 5.65×10^{-14} M and a limit of quantification (LOQ) of 1.88×10^{-13} M. Selectivity studies demonstrated negligible interference even in the presence of a 1000-fold excess of structurally related compounds. The method was successfully applied to commercial serum samples and pharmaceutical dosage forms, yielding recovery values of 98.61–99.82% and 99.60%, respectively. Furthermore, the practical applicability of the proposed sensor was validated by successfully CTZ in real biological samples and pharmaceutical formulations, highlighting its robustness and potential for real-sample analysis.

Keywords: Ceftazidime, Molecularly imprinted polymers, Drug analysis, Nanomaterials, Electrochemical sensors

I. INTRODUCTION

Ceftazidime (CTZ) is a third-generation cephalosporin characterized by broad-spectrum antibacterial activity, with high efficacy against a wide range of aerobic Gram-positive and Gram-negative microorganisms. It is particularly effective against Pseudomonas aeruginosa and other clinically significant Gram-negative pathogens, making it a widely prescribed agent for treating severe hospital- and community-acquired infections, including respiratory, urinary, bloodstream, and skin infections [1]. It is widely prescribed in clinical practice for the treatment of infectious conditions in both pediatric and adult populations. Nevertheless, in neonatal care, ceftazidime is frequently administered outside its approved indications, constituting an off-label use [2].

Numerous analytical techniques have been developed to determine CTZ, with chromatographic and spectroscopic methods being the most widely used. Among these, high-performance liquid chromatography (HPLC) [3,4] and ultra-performance liquid chromatography-mass spectrometry (UPLC–MS) [5,6] are widely used due to their high sensitivity and selectivity. In addition, infrared (IR) spectroscopy [7] and HPLC with ultraviolet detection (HPLC–UV) [8,9] have been widely used for the routine analysis of CTZ in pharmaceutical formulations and biological samples. Owing to their high sensitivity and strong analytical capability, these techniques have been extensively applied in CTZ analysis. Electrochemical degradation has been employed to study the breakdown of CTZ, while electroanalytical methods have been used to characterize the resulting products. These methods provide high sensitivity and reproducibility, allowing the detection and analysis of CTZ and its degradation products even in complex biological matrices [10–12].

Corresponding Author: AHMET ÇETİNKAYA, **Tel:** +90 544 343 50 07, **E-mail:** ahmet.cetinkya@yahoo.com

Submitted: 30.01.2026, **Revised:** 24.02.2026, **Accepted:** 10.03.2026

Conventional chromatographic and spectroscopic techniques, although highly precise, often require extensive sample preparation, prolonged analysis times, and costly instrumentation operated by trained personnel, which can limit their practical application in routine or point-of-care CTZ monitoring. In contrast, electrochemical methods have emerged as a promising alternative due to their cost-effectiveness, operational simplicity, rapid response, high sensitivity, and potential for miniaturization [13-15]. Nonetheless, standard electrochemical sensors may still face challenges, such as diminished selectivity in complex biological matrices and interference from structurally similar or electroactive compounds present in the sample [16-18]. To overcome these limitations, electrochemical platforms have been modified with molecularly imprinted polymers (MIPs), synthetic polymers engineered to contain a specific recognition site [19–21].

The integration of MIPs enhances the sensor's selectivity, reduces interference from coexisting substances, and maintains structural stability, while enabling a cost-effective, straightforward fabrication process [22–24]. During sensor preparation, CTZ is incorporated into the pre-polymerization mixture to generate complementary binding sites within the polymer network. After polymerization, the CTZ molecules are removed using an appropriate extraction procedure, leaving particular cavities that are both geometrically and chemically complementary to CTZ. These tailored recognition sites allow the polymer to selectively rebind CTZ in subsequent analyses, thereby improving the sensor’s specificity and overall analytical performance.

The analytical performance of MIP-based sensors can be substantially enhanced by integrating nanomaterials, which improve surface area, electrical conductivity, and overall sensitivity. Among these, graphene oxide-supported gold nanoparticles (GO@AuNPs) have attracted considerable attention due to their synergistic properties. The combination of graphene oxide (GO) and gold nanoparticles (AuNPs) provides a high surface-to-volume ratio, excellent electron transport, and numerous active sites, thereby enhancing the sensitivity of MIP-modified electrodes. GO provides a robust, conductive platform with abundant functional groups for polymer immobilization. At the same time, AuNPs facilitate rapid electron transfer and increase the density of binding sites within the imprinted polymer matrix. Consequently, GO@AuNP-modified MIP sensors exhibit superior performance in detecting trace amounts of target analytes in complex biological or environmental samples.

The incorporation of GO@AuNPs nanocomposites constitutes a strategic and rational approach to developing electrochemical sensors with enhanced sensitivity, improved selectivity, and excellent reproducibility, owing to their synergistic effects on electron-transfer efficiency, surface area, and signal amplification [25,30].

In this work, GO@AuNP–supported MIP–based electrochemical sensor was successfully fabricated for the sensitive and selective determination of CTZ. The MIP layer was formed directly on a bare glassy carbon electrode (GCE) via photopolymerization (PP), using trans-3-(3-pyridyl)acrylic acid (3,3-PAA) as the functional monomer. The integration of GO@AuNPs into the sensing interface significantly increased the effective surface area, improved electrical conductivity, and provided a higher density of accessible recognition sites. Furthermore, critical analytical parameters—including the template-to-monomer molar ratio, nanocomposite loading, and polymerization conditions—were systematically optimized to enhance imprinting efficiency and maximize overall electrochemical sensing performance. The surface morphology and microstructural features of MIP–modified electrodes were systematically examined by scanning electron microscopy (SEM) to monitor the formation and distribution of the imprinted polymer layer as well as the successful incorporation of the GO@AuNP nanocomposite. SEM analysis provided direct evidence of polymer film uniformity, surface roughness, and the presence of nanostructured features associated with the imprinted recognition sites. In addition, the electrochemical behavior of the MIP-based sensing interfaces was comprehensively evaluated using cyclic voltammetry (CV) and electrochemical impedance spectroscopy (EIS). CV measurements were used to investigate the redox activity and electron-transfer characteristics of the modified electrodes at each fabrication step, enabling assessment of changes in peak current associated with MIP layer formation and template removal. EIS analysis was used to quantitatively determine variations in interfacial charge-transfer resistance and capacitance arising from the imprinting process. The combined CV and EIS results provided critical insight into the influence of the MIP layer on mass transport, charge-transfer kinetics, and electron-transfer efficiency, thereby confirming the successful construction and functional performance of the MIP-based electrochemical sensor. Recovery studies were performed in both serum and pharmaceutical samples to demonstrate practical applicability, and selectivity experiments confirmed that the sensor could accurately detect CTZ even in the presence of structurally related cephalosporins, including cefazolin, cefdinir, cefixime, cefuroxime, and ceftriaxone. These characteristics indicate that the developed sensor is broadly applicable across diverse

sample matrices and analytical settings. Its high sensitivity, selectivity, and stability make it a reliable tool for the quantitative determination of ceftazidime in both biological and pharmaceutical samples. Consequently, the proposed sensor offers a promising and practical alternative to conventional analytical techniques, such as high-performance liquid chromatography (HPLC), liquid chromatography-tandem mass spectrometry (LC-MS/MS), and gas chromatography-mass spectrometry (GC-MS/MS), for routine monitoring and trace-level detection of target analytes [3-9, 31-34].

II. MATERIAL AND METHOD

2.1. Reagents and Chemicals

Stock solutions of CTZ (97.5%), and structurally related cephalosporins—cefazolin (≥97.0%), cefdinir (≥97.0%), cefixime (≥98.0%), cefuroxime (≥97.0%), and ceftriaxone (99.9%)—were prepared using methanol (MeOH, ≥99.8%) as the solvent. Sodium hydroxide (NaOH, >97.0%), acetic acid (HAc, ≥99.0%), 2-hydroxyethyl methacrylate (HEMA, ≥99%), acetonitrile (ACN, ≥99.9%), hydrochloric acid (37.0%), acetone (≥99.5%), 2-hydroxy-2-methyl propiophenone (≥97%), potassium ferricyanide ($K_3[Fe(CN)_6]$, ≥98.5%), 3,3-PAA (≥97%), potassium ferrocyanide ($K_4[Fe(CN)_6]$, ≥99.0%), graphene oxide nanoparticles (GO, 2 mg mL^{-1}, dispersion in H_2O), and gold nanoparticles (5 nm diameter, suspension in citrate buffer) were also obtained from Merck (Darmstadt, Germany). Additional reagents, including ethanol (EtOH, ≥99.0%), magnesium chloride ($MgCl_2$, ≥99.0%), potassium nitrate (KNO_3, ≥99.0%), sodium sulfate (Na_2SO_4, ≥99.0%), as well as paracetamol (PAR, ≥99.0%), ascorbic acid (AA, ≥99.0%), uric acid (UA, ≥99.0%), dopamine (DOP, ≥99.0%), and commercially available human serum samples used for real-sample applications, were supplied by Sigma-Aldrich (Darmstadt, Germany). Unless otherwise stated, all chemicals and prepared solutions were stored under refrigerated conditions.

2.2. Equipment and Apparatus

All chemicals were accurately weighed using a high-precision analytical balance (Ohaus Instruments, Shanghai, China). The pH of each prepared solution was measured with a calibrated pH/ion meter (Mettler-Toledo S220, Switzerland). The MIP layer was synthesized via PP using a 100 W 365 nm UV lamp. Electrochemical fabrication steps and measurements were performed in a standard three-electrode system comprising a glassy carbon electrode (GCE, 3.0 mm diameter) as the working electrode, a platinum wire as the auxiliary electrode, and an Ag/AgCl (3.0 M KCl) electrode as the reference. CV, DPV, and EIS analyses were performed using an AUTOLAB potentiostat/galvanostat with Nova 2.1.7 software (Metrohm, Netherlands). A thermo-shaker (Biosan TS-100) was used during template extraction and rebinding to ensure consistent interaction conditions. Homogeneous dispersion and effective mixing of solutions were achieved using an ultrasonic bath (JP Selecta Corporation, Barcelona, Spain) and a vortex mixer (ISOLAB Laborgeräte GmbH, Germany). The surface morphology of the modified electrodes was examined by scanning electron microscopy (SEM) employing a TESCAN GAIA 3 system (Brno-Kohoutovice, Czech Republic).

2.3. Production of the CTZ/3,3-PA/GO@AuNPs/MIP-GCE and Non-imprinted Polymer (NIP)-Based Electrochemical Sensor

Prior to surface modification, the glassy carbon electrode (GCE) was placed in a 1.5 mL Eppendorf tube containing a 1:1 (v/v) methanol–distilled water mixture and sonicated for 15 min to remove surface contaminants. The electrode surface was carefully prepared by mechanical polishing using a fine alumina slurry applied on a polishing cloth. This process effectively removed surface irregularities and contaminants, resulting in a smooth and uniform surface essential for reproducible electrochemical measurements. Following polishing, the electrode was thoroughly rinsed with distilled water to eliminate any residual alumina particles and debris, ensuring a clean surface for subsequent experimental procedures.

Sensor fabrication commenced with the preparation of a prepolymerization solution. Initially, 20 µL of the template molecule CTZ (1.0 mM) was combined with 40 µL of the functional monomer 3,3-PAA (1.0 mM) to facilitate specific non-covalent interactions between the template and monomer units. Subsequently, 20 µL of GO@AuNPs dispersion was incorporated to introduce the nanocomposite component, thereby improving the electrode's electrical conductivity, surface area, and electron transfer kinetics. Then, 100 µL of 2-hydroxyethyl methacrylate (HEMA) was added as the basic monomer to form the polymeric matrix, and 20 µL of ethylene glycol dimethacrylate (EGDMA) was included as a crosslinker to reinforce the structural integrity and stability of the resulting polymer network. The resulting solution was sonicated for 15 min to achieve homogeneous dispersion, after which 2 µL of 2-hydroxy-2-methylpropiophenone was introduced as the photoinitiator. A precisely measured 0.50 µL aliquot of the prepolymerization mixture was drop-cast onto the cleaned GCE surface. The PP step was performed by placing the coated electrode under a UV lamp operating at 365 nm with an output power of 100 W, maintaining it under continuous irradiation for 10 min at ambient conditions. Following the UV treatment, the electrode was removed from beneath the UV lamp and allowed to stand at room temperature for an additional 15 min to achieve thermal stabilization before further characterization and analytical measurements. After polymerization, the modified electrode was rinsed with distilled water, and the template molecules were removed, generating

specific recognition cavities. The rebinding process was subsequently carried out by incubating the MIP-modified electrode in a CTZ solution of known concentration using a thermo-shaker at 25 °C and 500 rpm for 10 min, allowing selective reoccupation of the imprinted sites. The schematic illustration of the sensor's production stages is shown in Scheme 1.

The electrochemical behavior of the electrode at different fabrication stages—including the bare GCE, after polymer formation and template removal, and following rebinding—was evaluated using a 5.0 mM $[Fe(CN)_6]^{3-/4-}$ redox probe. For comparison and control, a non-imprinted polymer (NIP) electrode was fabricated under identical conditions, excluding the template molecule from the prepolymerization mixture.

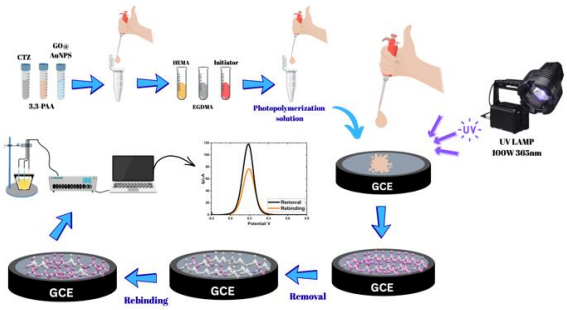

Scheme 1. Schematic representation of the production stages of the developed sensor

2.4. The Commercial Serum and Pharmaceutical Dosage Forms Applications

Commercially obtained serum samples were stored at −20 °C prior to analysis to preserve sample integrity. Serum stock solutions were prepared using a protein precipitation protocol to minimize matrix interferences. Briefly, 3.6 mL of human serum was mixed with 5.4 mL of acetonitrile (ACN) as a precipitating agent, then spiked with 1 mL of a standard CTZ solution to achieve the desired analyte concentration. The resulting mixture was subjected to ultrasonic treatment for 15 min to ensure thorough homogenization and efficient protein denaturation. Subsequently, the sample was centrifuged at 5000 rpm for 25 min to facilitate the complete separation of precipitated proteins. After centrifugation, the clear supernatant was carefully collected and directly used for subsequent electrochemical measurements. Method validation and recovery assessments were conducted by spiking treated serum samples with known concentrations of CTZ, and analyte quantification was performed using the regression equation derived from the calibration curve.

For the pharmaceutical dosage form, commercially available CTZ (1000 mg per unit) was finely pulverized using a mortar and pestle to ensure uniformity. An accurately weighed quantity of the sample, corresponding to the amount necessary to obtain a 1 mM solution, was transferred into a 10 mL volumetric flask and dissolved in methanol (MeOH). The resulting suspension was sonicated in a water bath for 30 min to achieve complete dissolution and uniform dispersion.

CTZ concentrations were quantified within the calibration curve's linear range, and spiking samples containing known amounts of the standard analyte were used to determine recovery. CTZ concentrations were determined using a calibration curve, and analytical precision was assessed by calculating relative standard deviations (RSDs) from five independent replicates at each concentration.

III. RESULT AND DISCUSSION

3.1. Surface Characterization of CTZ/3,3-PA/GO@AuNPs/MIP-GCE Sensor

SEM was used to systematically examine the surface morphology of the CTZ/3,3-PAA/GO@AuNPs/MIP-GCE sensor at 20.00 KX magnification to evaluate the impact of molecular imprinting on electrode topography. The SEM images revealed that the MIP-modified electrode exhibited a distinctly rough, highly porous structure, characterized by numerous cavities and channels indicative of successful template imprinting and providing sites for selective CTZ recognition (Figure 1A). In contrast, the non-imprinted polymer (NIP) electrode exhibited a comparatively smooth, compact surface, lacking the microcavities required for specific molecular interactions, underscoring the critical role of imprinting in creating selective binding sites (Figure 1B). These morphological differences confirm that incorporating GO@AuNPs not only enhances the electrode's surface area but also contributes to the formation of a three-dimensional porous network, which is favorable for target molecule accessibility and efficient electrochemical response.

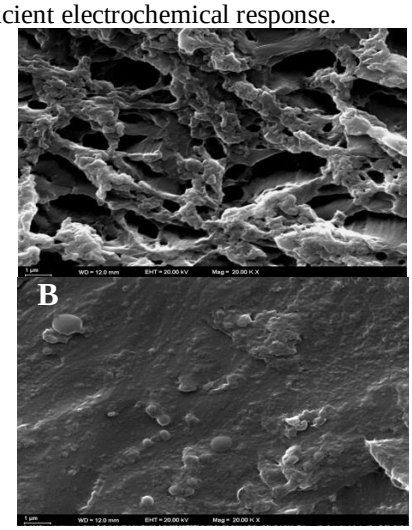

Figure 1. The modified electrode's surface morphology characterization images obtained using SEM of CTZ/3,3-PA/GO@AuNPs/MIP-GCE (A) and CTZ/3,3-PA/GO@AuNPs/NIP-GCE (B) surfaces.

3.2. Electrochemical Characterization of CTZ/3,3-PA/GO@AuNPs/MIP-GCE Sensor

The electron transfer properties of the CTZ/3,3-PAA/GO@AuNPs/MIP-GCE sensor were evaluated by CV in successive stages of sensor fabrication: bare GCE, after PP, after removal, and rebinding of CTZ molecules. As shown in Figure 2A, bare GCE exhibited the highest current responses, reflecting unimpeded electron transfer in the absence of a polymeric layer. Deposition of the MIP film significantly suppressed redox peak currents due to the insulating nature of the polymer matrix. Subsequent removal of the CTZ template created selective binding vacancies, facilitating electron transfer and increasing peak currents. With the re-addition of CTZ molecules, these complementary vacancies were reoccupied, leading to a significant decrease in current signals. The observed cyclic modulation of the CV responses confirms the successful formation of the molecularly imprinted polymer and its selective recognition of CTZ. The electron transfer resistance (Rct) at each stage of sensor modification was evaluated using Nyquist plots obtained from EIS measurements in a 5.0 mM $[Fe(CN)_6]^{3-/4-}$ redox probe solution (Figure 2B). The bare GCE exhibited the smallest semicircular Rct (130 Ω), indicating efficient electron transfer and minimal resistance. After PP, the insulating layer hindered electron movement, resulting in a significant increase in Rct (4960 Ω), reflected by the most enormous semicircle. Removal of the CTZ created accessible cavities, facilitating electron transfer and resulting in a smaller semicircle (530 Ω). Upon CTZ rebinding, Rct (986 Ω) increased again, suggesting partial cavity occupation; however, the resistance remained lower than that observed after PP. These results confirm the successful fabrication of the CTZ/3,3-PAA/GO@AuNPs/MIP-GCE sensor and demonstrate its ability to modulate electron-transfer properties through selective molecular recognition of CTZ.

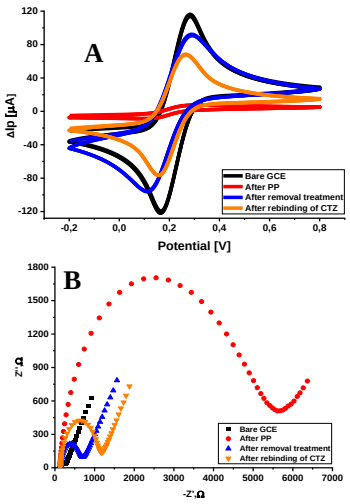

Figure 2. Electrochemical characterization of the designed CTZ/3,3-PA/GO@AuNPs/MIP-GCE sensor: (A) cyclic voltammograms, (B) EIS, Nyquist plots.

3.3. Optimization Parameters

3.3.1. Nanomaterial Effect on MIP-Based Sensor

The initial stage in optimizing the CTZ/3,3-PA/GO@AuNPs/MIP-GCE sensor focused on identifying a suitable nanomaterial to improve its performance. Nanomaterial-supported MIP sensors are well known for their enhanced analytical capabilities, owing to their large surface area, improved electron-transfer efficiency, and excellent physical and chemical stability. In this work, a variety of nanoparticles—including GO, AuNPs, silver nanoparticles (AgNPs), zinc oxide nanoparticles (ZnONPs), titanium dioxide nanoparticles (TiO_2NPs), copper nanoparticles (CuNPs), and GO@AuNPs composites—were systematically tested to assess their influence on sensor response. Performance evaluation was performed by measuring the current difference (ΔIp_2) after removal and subsequent rebinding of CTZ molecules. Among all tested materials, GO@AuNPs yielded the highest peak currents, demonstrating the greatest signal enhancement, and were therefore chosen for electrode modification. The maximum ΔIp_2 was observed at GO@AuNPs, indicating that it provided sufficient surface coverage and facilitated efficient electron transfer without causing aggregation or obstructing the electrode surface (**Figure 3**). This optimization improved the sensor's sensitivity and its ability to selectively recognize CTZ in complex matrices.

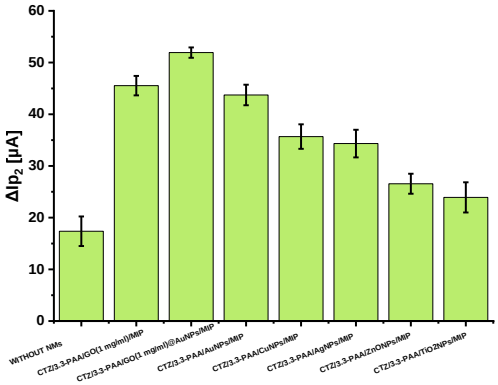

Figure 3. The effect of GO@AuNPs nanomaterial on CTZ/3,3-PA/GO@AuNPs/MIP-GCE sensor

3.3.2. Template-to-Monomer Ratio

The stoichiometric relationship between the template molecule and the functional monomer is critical to MIP sensor fabrication, as it governs the formation and performance of the imprinted polymer network. An optimal ratio ensures the formation of sufficiently high-fidelity binding sites that are complementary in shape and chemical functionality to the template molecule, thereby enhancing both the selectivity and sensitivity of the sensor. Deviations from this ratio can lead to incomplete template-monomer interactions, resulting in fewer or poorly defined cavities, which adversely affect the sensor's recognition capability and overall analytical performance.

Therefore, careful adjustment and optimization of the template-to-monomer ratio are essential to achieve reproducible polymerization and maximize the sensor's binding efficiency. An optimal template-to-monomer ratio ensures that sufficient functional monomers are available to interact with the template, resulting in well-defined, highly specific recognition sites. If the monomer concentration is too low relative to the template, the resulting binding sites may be incomplete or weak, reducing the sensor's sensitivity and affinity. Conversely, an excessive amount of monomer can lead to an overly dense or disordered polymer network, which may promote nonspecific interactions and reduce selectivity. In this study, CTZ was used as the template molecule, and 3,3-PAA served as the functional monomer. Various CTZ-to-3,3-PAA ratios (1:1, 1:2, 1:3, 1:4, and 1:5) were tested, and ΔIp_1 values were calculated by comparing the peak current differences of CTZ before and after template removal. The highest response and optimal performance were achieved at a 1:3 CTZ-to-3,3-PAA ratio, which was subsequently used to prepare the polymerization solution for all subsequent experiments (Figure 3A).

3.3.3. Dropping Volume

The efficiency and uniformity of the polymerization process are critically dependent on the volume of the monomer solution applied to the glassy carbon electrode (GCE) surface. The applied volume directly governs the thickness and morphology of the resulting polymer film, which in turn influences the accessibility of binding sites, electron-transfer kinetics, and overall sensor responsiveness. Thicker films, typically formed from larger drop volumes, can increase the density of recognition sites but may impede analyte diffusion and slow charge-transfer processes, whereas thinner films generated from smaller volumes facilitate rapid mass transport and efficient electron transfer but may reduce the number of available binding cavities. In the present study, a series of drop volumes ranging from 0.25 to 1.25 μL were systematically investigated to assess their impact on the electrochemical performance of the sensor (Figure 3B). The results showed that ΔIp_1 values varied with the applied volume, reaching a maximum at 0.50 μL. Beyond this volume, further increases led to a gradual decrease in ΔI_1, likely due to the formation of excessively thick films that hinder electron transfer. Therefore, a drop volume of 0.50 μL was selected as optimal and consistently used in all subsequent experiments.

3.3.4. PP Time

Optimizing PP time is crucial for achieving effective polymer formation. In this study, the PP duration was systematically varied at 5, 7, 10, 12, and 15 min under UV irradiation to determine the conditions that maximize polymerization efficiency.

The ΔIp_1 values were monitored to evaluate sensor performance at the PP time point (Figure 3C). The results indicated that a PP time of 7 min provided the highest and most reproducible response, making it the optimal duration for the polymerization process.

3.3.5. Removal Solution and Removal Time

To create specific recognition sites, the removal of the template molecule must be carefully optimized. This step disrupts the non-covalent interactions formed between CTZ and 3,3-PAA during polymerization. For the CTZ/3,3-PA/GO@AuNPs/MIP-GCE sensor, template extraction was carried out using a Thermo-Shaker set at 650 rpm with several potential solvents, including 10 M and 15 M HAc, MeOH, 1 M HCl, 1 M NaOH, acetone, and ACN. The effectiveness of each solvent was evaluated by monitoring ΔIp1, which reflects the efficiency of CTZ removal. Among the tested solvents, 15 M HAc provided the most complete template extraction (Figure 3D). Using this optimized solvent, the effect of extraction time was investigated over 5-15 min. The results showed that ΔI_1 values stabilized after 12 min, indicating that this duration was sufficient for complete removal. Consequently, 15 M HAc for 12 min was determined to be the optimal extraction condition for preparing the CTZ-specific MIP sensor (Figure 3E).

3.3.6. Rebinding Time

The final step in optimizing the CTZ/3,3-PA/GO@AuNPs/MIP-GCE sensor involved determining the optimal binding time for CTZ. To investigate this, the modified electrode was immersed in a 1.0×10^{-11} M CTZ solution in ultrapure water and agitated at 650 rpm using a Thermo-Shaker. The ΔIp_2 values, defined as the difference in peak current before and after CTZ rebinding, were measured at 5-15 min intervals (Figure 3F). The results indicated a gradual increase in ΔI_2 up to 15 min, reflecting more complete rebinding of CTZ to the polymeric recognition sites. No further enhancement was observed beyond this period, suggesting that prolonged incubation does not improve binding efficiency and may slightly affect the integrity of the polymer matrix. Consequently, a binding time of 15 min was determined to be optimal for CTZ interaction with the sensor.

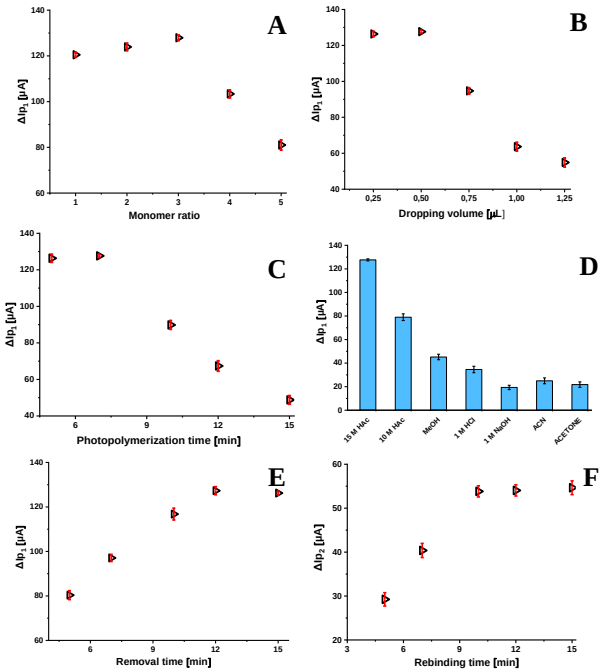

Figure 4. Optimization of (A) Monomer/Template Ratio, (B) Dropping volume, (C) PP time, (D) Removal solutions, (E) Removal time, (F) Rebinding time of CTZ/3,3-PA/GO@AuNPs/MIP-GCE in 5 mM $[Fe(CN)_6]^{3-/4-}$ solution (0.1 M KCl).

3.4. Analytical Evaluation of CTZ/3,3-PA/GO@AuNPs/MIP-GCE Sensor in Standard Solution

The analytical response of the CTZ/3,3-PA/GO@AuNPs/MIP-GCE sensor was evaluated in standard solutions following the optimization of all experimental conditions. DPV measurements were recorded after the rebinding of increasing CTZ concentrations ranging from 2.50×10^{-13} to 3.75×10^{-12} M (Figure 5A). The voltammograms showed a gradual decrease in the redox probe's peak current as the CTZ concentration increased. Correspondingly, the ΔI_2 values, calculated by subtracting the peak currents after CTZ rebinding from those after template removal, increased linearly with concentration. The calibration curve is shown in Figure 5B, with an excellent correlation coefficient (r = 0.997) and the linear regression equation:

$$\Delta I_2\,(\mu A) = 4.06 \times 10^{11} \times C\,(M) + 26.52 \quad (r = 0.997)$$

The regression parameters are summarized in Table 1. The sensor response saturated above the specified linear range, whereas lower concentrations yielded negligible binding. The limit of detection (LOD) and limit of quantification (LOQ) were calculated according to the guidelines provided by the International Council for Harmonisation (ICH) [35,36].

$$LOD = \frac{3 \times Standard\ Deviation}{Slope}$$

$$LOQ = \frac{10 \times Standard\ Deviation}{Slope}$$

Using the calibration data, the LOD and LOQ for the CTZ/3,3-PA/GO@AuNPs/MIP-GCE sensor were determined according to ICH guidelines, yielding 5.65×10^{-14} M and 1.88×10^{-13} M, respectively. These findings highlight the sensor's remarkable sensitivity and its strong ability to reliably quantify CTZ at trace concentrations.

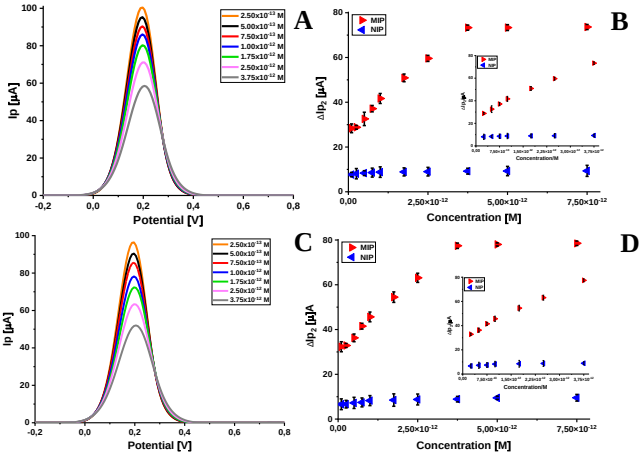

Figure 5. DP voltammograms after rebinding of CTZ on CTZ/3,3-PA/GO@AuNPs/MIP-GCE (A), and the calibration line (B) in standard CTZ solutions. DP voltammograms after rebinding of CTZ on CTZ/3,3-PA/GO@AuNPs/MIP-GCE (C), and the calibration line (D) in commercial serum samples.

Table 1. Regression data of the calibration line for CTZ/3,3-PA/GO@AuNPs/MIP-GCE

	Standard solution	**Commercial serum sample**
Linearity range (M)	2.50×10^{-13} – 3.75×10^{-12}	2.50×10^{-13} – 3.75×10^{-12}
Slope (µA M^{-1})	1.27×10^{13}	1.26×10^{13}
SE of slope	4.06×10^{11}	3.77×10^{11}
Intercept (µA)	26.52	30.61
SE of intercept	0.80	0.71
Correlation coefficient (*r*)	0.997	0.996
LOD (M)	5.65×10^{-14}	7.17×10^{-14}
LOQ (M)	1.88×10^{-13}	2.39×10^{-13}
Repeatability of peak current (RSD%)*	0.83	0.94
Reproducibility of peak current (RSD%)*	1.12	1.86

*Each value is the mean of three experiments.

3.5. Application of CTZ/3,3-PA/GO@AuNPs/MIP-GCE Sensor on Real Samples

The applicability of the CTZ/3,3-PA/GO@AuNPs/MIP-GCE sensor in complex matrices was investigated by spiking known concentrations of CTZ into commercial serum samples. DPV measurements revealed a linear increase in ΔIp_2 with CTZ concentration over the range of 2.50×10^{-13} to 3.75×10^{-12} M, indicating effective quantitative detection in these complex matrices (Figure 5D). The regression equation described the corresponding calibration curve:

$$\Delta Ip_2\ (\mu A) = 3.777 \times 10^{11}\ C\ (M) + 30.61\ (r = 0.996)$$

From these data, the LOD and LOQ were calculated to be 7.17×10^{-14} M and 2.39×10^{-13} M, respectively (Table 1). The DP voltammograms (Figure 5C) showed a progressive decrease in peak current as the imprinted cavities were gradually occupied by CTZ molecules, reflecting the sensor's selective recognition mechanism. These findings confirm that the CTZ/3,3-PA/GO@AuNPs/MIP-GCE sensor exhibits excellent sensitivity, reproducibility, and suitability for CTZ detection in biological samples.

Recovery experiments were carried out using commercial serum samples to assess the performance of the CTZ/3,3-PA/GO@AuNPs/MIP-GCE sensor in complex biological matrices. Known concentrations of CTZ were spiked into the serum at three different levels, and DPV measurements were recorded for each sample. The calculated recoveries indicated that endogenous serum components did not significantly affect the sensor response. Furthermore, the relative standard deviation (RSD) values were within

acceptable limits, demonstrating the method's high reproducibility and sensitivity.

The practical applicability of the developed sensor was evaluated using a commercially available CTZ pharmaceutical dosage form. Recovery studies were performed by adding known amounts of CTZ to the formulation, allowing assessment of potential interference from excipients. The results showed that the presence of excipients did not affect the sensor's electrochemical response, confirming its high selectivity and reliability for the accurate quantification of CTZ in pharmaceutical preparations (Tables 2 and 3).

Table 2. Recovery study results for commercial serum samples

	Commercial serum sample		
Sample concentration (M)	5.00×10^{-13}	7.50×10^{-13}	1.00×10^{-12}
Spiked amount (M)	1.25×10^{-12}	1.00×10^{-12}	0.75×10^{-12}
Found amount (M)*	1.71×10^{-12}	1.74×10^{-12}	1.72×10^{-12}
Average recovery (%)*	99.82	99.63	98.61
RSD% of recovery	1.58	2.96	2.39
Bias%	+0.18	+0.37	+1.39

*Each value is the mean of five experiments.

Table 3. Recovery experiment results for pharmaceutical dosage forms

	Pharmaceutical dosage forms
Label amount (mg)	1000.00
Found amount (mg)*	1003.00
RSD%	0.78
Spiked amount (mg)	100.00
Found amount (mg)*	1100.30
Average recovery (%)*	99.60
RSD%	1.25
Bias%	+0.40

*Each value is the mean of five experiments.

3.6. Selectivity and Specificity Studies and Imprinting Factor

The imprinting factor (IF) is a key metric for evaluating the performance of an MIP sensor, as it quantitatively reflects the MIP's enhanced recognition capability and binding specificity relative to a corresponding NIP. Higher IF values indicate more successful imprinting, resulting in enhanced selectivity, improved sensitivity, and better reproducibility of the sensor. A central aim of MIP design is to achieve selective recognition of the target molecule even in the presence of structurally similar compounds. The selectivity of the CTZ/3,3-PA/GO@AuNPs/MIP-GCE sensor was assessed by testing its electrochemical response in the presence of multiple competing antibiotics—cefuroxime, cefazolin, cefdinir, cefixime, ceftazidime, and ceftriaxone—at concentrations comparable to CTZ. The negligible interference observed confirmed the sensor's excellent discrimination capability and its suitability for selective CTZ detection in complex samples.

The binding specificity of the sensor was quantitatively assessed using the selectivity coefficient (k) and the relative selectivity coefficient (k′).

These parameters provide a numerical measure of the sensor's preferential recognition of CTZ over structurally related cephalosporin antibiotics, thereby offering a robust evaluation of its selectivity and molecular imprinting efficiency. The relevant calculations for IF, k, and k′ are provided in the following equations, serving as the basis for the selectivity evaluation.

$$k_{(MIP)} = \frac{\Delta I_2(MIP)\ for\ CTZ}{\Delta I_2(MIP)\ for\ other\ drug}$$

$$k_{(NIP)} = \frac{\Delta I_2(NIP)\ for\ CTZ}{\Delta I_2(NIP)\ for\ other\ drug}$$

$$k' = \frac{k_{(MIP)}}{k_{(NIP)}}$$

Compared with these other compounds, the developed MIP sensor exhibited significantly higher selectivity toward CTZ, approximately 4 times that of the other antibiotics (Table 4).

Table 4. Specificity results of CTZ/3,3-PA/GO@AuNPs/MIP-GCE with 1000-fold higher concentration of similarly structured molecules

Molecules	MIP/GCE		NIP/GCE		
	$\Delta I_2/\mu A$	$k_{(MIP)}$	$\Delta I_2/\mu A$	$k_{(NIP)}$	$k'_{(MIP/NIP)}$
CTZ	43,79	–	8,47	–	**–**
Cefazolin	6,97	6,28	5,78	1,46	**4,28**
Cefdinir	8,28	5,28	6,54	1,29	**4,08**
Cefixime	8,05	5,43	6,57	1,28	**4,21**
Cefuroxime	7,99	5,48	6,37	1,32	**4,12**
Ceftriaxone	7,02	5,52	6,72	1,26	**4,38**

Evaluating possible interfering species in biological matrices is essential to confirm that the sensor maintains high selectivity toward the target analyte.

A systematic evaluation of the sensor's analytical performance was conducted by investigating its electrochemical response in the presence of various potential interfering species commonly encountered in biological fluids.

These species included inorganic ions (K^+, Na^+, Cl^-, SO_4^{2-}, Mg^{2+}, and NO_3^-) and electroactive organic compounds of physiological relevance, such as dopamine (DOP), ascorbic acid (AA), uric acid (UA), and paracetamol (PAR). The selectivity of the CTZ/3,3-PA/GO@AuNPs/MIP-GCE sensor was rigorously evaluated using DPV. Potential interfering species, including common inorganic ions and electroactive biomolecules, were introduced at 1000-fold higher concentrations than CTZ to create interference conditions. The resulting electrochemical responses were recorded, and the corresponding recovery % and RSD% values were calculated to quantitatively assess the sensor's ability to distinguish CTZ from structurally similar or electroactive compounds (Figure 6). The results demonstrate that none of the species examined caused significant interference, confirming that the sensor exhibits excellent selectivity for CTZ determination.

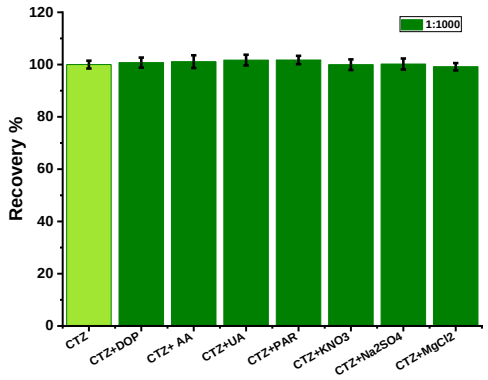

Figure 6. Structures of the molecules; Graphs of recovery results obtained using 1.00×10^{-12} M CTZ tested with the designed CTZ/3,3-PA/GO@AuNPs/MIP-GCE sensor in the presence of interfering agents at a 1:1000 ratio.

3.7. Comparison of Selected Analytical Methods

A comprehensive review of the existing literature reveals several disadvantages of chromatographic and spectroscopic approaches used for CTZ determination. These methodologies generally require large volumes of organic solvents, involve complex, labor-intensive sample pretreatment steps, and require long analysis times. Furthermore, the use of advanced instrumentation significantly increases operating and maintenance costs, limiting its suitability for routine and high-throughput analyses. In contrast, the newly developed CTZ/3,3-PA/GO@AuNPs/MIP-GCE sensor offers a robust and efficient alternative for the selective determination of the target molecule CTZ. The integration of molecular imprinting technology with conductive nanomaterials enhances the specificity of recognition sites while simultaneously improving electron transfer kinetics. The sensor exhibits superior analytical performance, including high sensitivity and selectivity. In addition, the fabrication and operating procedures are relatively simple, reducing analysis time and minimizing reagent consumption, thereby contributing to both cost-effectiveness and environmental sustainability.

According to the comparative data presented in Table 5, the proposed sensor exhibits a wide linear dynamic range, high repeatability, and particularly low detection limits when compared to many conventional analytical techniques. These performance characteristics highlight its strong potential as a reliable, accurate, and practical platform for CTZ analysis in various application areas.

Table 5. Comparison of previous studies on CTZ determination with this study

Method	Linear Range	LOD	Sample	Recovery (%)	Ref.
HPLC	0.3-500 µg/mL	0.3 µg/mL	Serum	95.80	[3]
UHPLC-UV	2.0-100 mg/L	NA	Blood	73.90-99.50	[4]
UHPLC–MS/MS	0.1-5.0 mg/L	NA	Serum Urine Cerebrospinal fluid	90.00-106.00 76.00-92.00 106.00-116.00	[5]
UHPLC	0.5-32.0 mg/L	0.06 mg/L	Plasma	NA	[6]
IR	0.5-7.0 mg	NA	Pharmaceutical form	98.33-99.72	[7]
UV	7.0-14.0 µg/mL	NA	Serum	105.00-120.00	[8]
RP-HPLC	0.1-100 µg/mL	NA	Frog plasma	87.00-91.00	[9]
CTZ/3,3-PA/GO@AuNPs/MIP-GCE	**2.50×10^{-13}-3.75×10^{-12} M**	**5.65×10^{-14} M**	**Serum Pharmaceutical dosage form**	**98.61-99.82 99.60**	**This study**

IV. CONCLUSION

A nanocomposite-based electrochemical sensing platform (CTZ/3,3-PA/GO@AuNPs/MIP-GCE) was developed for the sensitive and selective electrochemical detection of CTZ. The synergistic integration of GO@AuNPs within the MIP framework resulted in a marked enhancement of electrochemical response due to improved interfacial conductivity, accelerated charge-transfer processes, and an expanded electroactive surface area, leading to superior analytical performance. Owing to this advanced design, the proposed sensor enabled rapid, user-friendly analysis of both standard solutions and serum samples. Under optimized conditions, CTZ was quantitatively detected with excellent sensitivity across a wide linear concentration range of 2.50×10^{-13} to 3.75×10^{-12} M, while a low limit of detection of 5.65×10^{-14} M was achieved in standard solutions.

The sensor's superior analytical performance can be attributed to the synergistic effect of GO@AuNPs and the molecularly imprinted polymer structure. The highly conductive GO@AuNPs framework accelerates electron transfer processes, resulting in enhanced signal intensity, while the tailor-made recognition cavities within the MIP layer facilitate selective binding of CTZ, thereby improving both sensitivity and selectivity. Furthermore, these selective cavities, explicitly designed for the target analyte, significantly enhance analyte recognition and binding efficiency, further boosting the sensor's analytical performance. The synergistic interaction between the conductive nanocomposite and the molecularly imprinted framework enables the sensor to operate with high accuracy and reliability, even in complex sample matrices. Consequently, the developed sensor provides a rapid, simple, and robust analytical approach that combines high sensitivity, selectivity, and reproducibility. These characteristics make it a highly suitable and reliable tool not only for quantifying active pharmaceutical ingredients in dosage forms but also for trace-level detection of analytes in complex biological and environmental samples, demonstrating its potential as an effective alternative for practical analytical applications.

REFERENCES

[1] Rains, C. P., Bryson, H. M., & Peters, D. H. (1995). Ceftazidime: An update of its antibacterial activity, pharmacokinetic properties and therapeutic efficacy. Journal of Pharmaceutical and Biomedical Analysis, 49(4), 577–617.

[2] Kontou, A., Kourti, M., Iosifidis, E., Sarafidis, K., & Roilides, E. (2023). Use of newer and repurposed antibiotics against gram-negative bacteria in neonates. Antibiotics, 12(6), 1072.

[3] Myers, C. M., & Blumer, J. L. (1983). Determination of ceftazidime in biological fluids by using high-pressure liquid chromatography. Antimicrobial Agents and Chemotherapy, 24(3), 343–346.

[4] Legrand, T., Vodovar, D., Tournier, N., Khoudour, N., & Hulin, A. (2016). Simultaneous determination of eight β-lactam antibiotics in human plasma by ultra-high-performance liquid chromatography with ultraviolet detection. Antimicrobial Agents and Chemotherapy, 60(8), 4734–4742.

[5] Cazorla-Reyes, R., Romero-González, R., Frenich, A. G., Maresca, M. A. R., & Vidal, J. L. M. (2014). Simultaneous analysis of antibiotics in biological samples by ultra-high-performance liquid chromatography–tandem mass spectrometry. Journal of Pharmaceutical and Biomedical Analysis, 89, 203–212.

[6] Lefeuvre, S., Bois-Maublanc, J., Hocqueloux, L., Bret, L., Francia, T., et al. (2017). A simple ultra-high-performance liquid chromatography–high resolution mass spectrometry assay for the simultaneous quantification of 15 antibiotics in plasma. Journal of Chromatography B, 1065, 50–58.

[7] de Haro Moreno, A., & Salgado, H. R. N. (2012). Development and validation of the quantitative analysis of ceftazidime in powder for injection by infrared spectroscopy. Physical Chemistry, 2, 6–11.

[8] de Haro Moreno, A., & Salgado, H. R. N. (2009). Rapid and selective UV spectrophotometric method for the analysis of ceftazidime. Journal of AOAC International, 92(3), 820–823.

[9] Bergman, J., Harvill, L., Hawkins, S., Sladky, K., & Cox, S. (2021). Determination of ceftazidime in plasma by RP-HPLC and ultraviolet detection. Biomedical Chromatography, 35(7), e5104.

[10] Xie, T., Wang, L., Wang, H., Cao, C., Tang, C., et al. (2024). In-situ electrodeposition of Co/Ce-MOF-derived carbon composites as an anode for electrochemical degradation of ceftazidime. Separation and Purification Technology, 330, 125231.

[11] Ni, Y., Kang, Y., Liu, Y., Bi, W., Qin, J., et al. (2024). Fabrication and characterization of a novel Ce-modified PbO_2 electrode with Ti_4O_7-rGO as a middle layer for the degradation of ceftazidime. Desalination, 117645.

[12] Li, X., Duan, P., Lei, J., Sun, Z., & Hu, X. (2019). Fabrication of Ti/TiO_2/SnO_2-Sb-Cu electrode for enhancing electrochemical degradation of ceftazidime in aqueous solution. Journal of Electroanalytical Chemistry, 847, 113231.

[13] Scholz, F., Stojek, Z., Inzelt, G., et al. (2010). Electroanalytical Methods: Guide to experiments and applications (2nd ed.). Springer, Berlin, Heidelberg, XXVII, 359.

[14] Baig, N., Sajid, M., & Saleh, T. A. (2019). Recent trends in nanomaterial-modified electrodes for electroanalytical applications. TrAC - Trends in Analytical Chemistry, 111, 47–61.

[15] Zabihollahpoor, A., Rahimnejad, M., Najafpour-Darzi, G., & Moghadamnia, A. A. (2020). Recent advances in electroanalytical methods for the therapeutic monitoring of antiepileptic drugs: A comprehensive review. Journal of Pharmaceutical and Biomedical Analysis, 188, 113394.

[16] Chaudhary, M., Kumar, A., Devi, A., Singh, B. P., Malhotra, B. D., & Singhal, K. (2023). Prospects of nanostructure-based electrochemical sensors for drug detection: A review. Materials Advances, 4, 432–457.

[17] De Rycke, E., Stove, C., Dubruel, P., De Saeger, S., & Beloglazova, N. (2020). Recent developments in electrochemical detection of illicit drugs in diverse matrices. Biosensors and Bioelectronics, 169, 112579.

[18] Klimuntowski, M., Alam, M. M., Singh, G., & Howlader, M. M. R. (2020). Electrochemical sensing of cannabinoids in biofluids: A noninvasive tool for drug detection. ACS Sensors, 5(3), 620–636.

[19] Cetinkaya, A., Kaya, S. I., Corman, M. E., Karakaya, M., Atici, E. B., & Ozkan, S. A. (2022). A highly sensitive and selective electrochemical sensor based on computer-aided design of molecularly imprinted polymer for the determination of leflunomide. Microchemical Journal, 179, 107496.

[20] Piskin, E., Cetinkaya, A., Eryaman, Z., Karadurmus, L., Unal, M. A., et al. (2024). Development of ultra-sensitive and selective molecularly imprinted polymer-based electrochemical sensor for L-lactate detection. Microchemical Journal, 204, 111163.

[21] Yence, M., Cetinkaya, A., Çorman, M. E., Uzun, L., Caglayan, M. G., et al. (2023). Fabrication of molecularly imprinted electrochemical sensors for sensitive codeine detection. Microchemical Journal, 193, 109060.

[22] Çorman, M. E., Cetinkaya, A., Armutcu, C., Uzun, L., & Ozkan, S. A. (2023). Designing of ZnO nanoparticles-oriented interface imprinted electrochemical sensor for fluoxetine detection. Bioelectrochemistry, 152, 108411.

[23] Cetinkaya, A., Unal, M. A., Nazir, H., Corman, M. E., Uzun, L., et al. (2024). Development of borazine-assisted-oriented molecularly imprinted electrochemical sensor for the detection of umifenovir in serum and urine. Sensors and Actuators B: Chemical, 420, 136519.

[24] Cetinkaya, A., Unal, M. A., Nazır, H., Çorman, M. E., Uzun, L., & Ozkan, S. A. (2024). A comparative study of electropolymerization and photopolymerization for the determination of molnupiravir via molecularly imprinted polymers. Microchimica Acta, 191(5), 270.

[25] Li, X., Wang, X., Li, L., Duan, H., & Luo, C. (2015). Electrochemical sensor based on magnetic graphene oxide@gold nanoparticles–molecular imprinted polymers for determination of dibutyl phthalate. Talanta, 131, 354–360.

[26] Huang, Z., Liu, T., Geng, J., Zhang, S., Neha, Ye, M., & Sun, W. (2026). Molecularly imprinted electrochemical sensor based on AuNPs-nitrogen doped graphene-MXene nanocomposite for the detection of kanamycin in milk. Journal of Food Composition and Analysis, 108868.

[27] Deepa, J. R., Jyothish, B., Athira, V. S., Mini, S., Sree Remya, T. S., & Nair, A. A. (2025). Molecularly imprinted electrochemical sensor enhanced with functionalized gold nanoparticle/graphene oxide composite for ultra-selective detection of homocysteine. Microchemical Journal, 115310.

[28] Mani, A., & Anirudhan, T. S. (2024). Electrochemical sensing of cortisol by gold nanoparticle incorporated carboxylated graphene oxide based molecularly imprinted polymer. Chemical Engineering Journal, 152654.

[29] Zhong, Y., Li, Z., Zhang, A., Peng, Y., Zhou, H., et al. (2024). Gold nanoparticle mediated molecularly imprinted electrochemical sensor for detection of neutral phosmet residues. Microchemical Journal, 201, 110728.

[30] Mani, A., & Anirudhan, T. S. (2024). Electrochemical sensing of cortisol by gold nanoparticle incorporated carboxylated graphene oxide based molecularly imprinted polymer. Chemical Engineering Journal, 493, 152654.

[31] Chauhan, V., Sharma, M., Tiwari, A., & et al. (2024). Developing, validating, and comparing an analytical method to simultaneously detect z-drugs in urine samples using the QuEChERS approach with both liquid chromatography and gas chromatography-tandem mass spectrometry. Saudi Pharmaceutical Journal, 32(2), 101950.

[32] Honert, C., Wifling, K., Lazo Hernández, M. J., & al. (2025). Assessment of current use pesticides in flowers, pollen provision, and wild bees: HPLC-ESI-MS/MS method development and field implementation. Analytical and Bioanalytical Chemistry, 417, 4199-4213.

[33] Koziarska, M., Strzebońska, M., & Szalińska, E. (2025). Development and validation of a green/blue UHPLC-MS/MS method for trace pharmaceutical monitoring. Scientific Reports, 15, 15614.

[34] Askar, A. M., Al Ali, A. Y., Khalifa, M. K., Salem, A. A., Alkhuwaildi, B. M., & Shah, I. (2025). Rapid GC-MS method for screening seized drugs in forensic investigations: optimization and validation. Frontiers in Chemistry, 13, 1559279.

[35] A. Procedures, Guidance for Industry Q2B Validation of Analytical Procedures: Methodology, 20857, 301–827.

[36] Ozkan, S. A., Kauffmann, J.-M., & Zuman, P. (2015). Electroanalytical method validation in pharmaceutical analysis and Their Applications. In S.A. Ozkan, J.M. Kauffmann, P. Zuman (Eds) Electroanalysis in biomedical and pharmaceutical sciences, (1st ed., pp. 235-266). Springer, Berlin, Heidelberg.